

# Ruthenium Ion-Complexed Carbon Nitride Nanosheets with Peroxidase-Like Activity as a Ratiometric Fluorescence Probe for the Detection of Hydrogen Peroxide and Glucose

Wenfang Deng,<sup>a,b,‡</sup> Yi Peng,<sup>b,‡</sup> Hui Yang,<sup>a</sup> Yueming Tan,<sup>a,b,\*</sup> Ming Ma,<sup>a</sup> Qingji Xie,<sup>a</sup> and Shaowei Chen<sup>b,\*</sup>

<sup>a</sup> Key Laboratory of Chemical Biology and Traditional Chinese Medicine Research (Ministry of Education), College of Chemistry and Chemical Engineering, Hunan Normal University, Changsha, Hunan 410081, China

<sup>b</sup> Department of Chemistry and Biochemistry, University of California, 1156 High Street, Santa Cruz, CA 95064, USA

**ABSTRACT:** Detection of hydrogen peroxide is of great significance for clinical diagnosis and biomedical research. Ratiometric detection represents an effective method that is generally based on horseradish peroxidase. In the present study, ruthenium ion-complexed carbon nitride ( $\text{Ru-C}_3\text{N}_4$ ) nanosheets are found to serve as a peroxidase mimic and can catalyze the conversion of *o*-phenylenediamine to fluorescent 2,3-diaminophenazine in the presence of  $\text{H}_2\text{O}_2$ . The produced 2,3-diaminophenazine also results in apparent quenching of the  $\text{Ru-C}_3\text{N}_4$  photoluminescence due to the inner filter effect. These unique characteristics can be exploited for the construction of an effective, peroxidase-free ratiometric fluorescence framework for the detection of  $\text{H}_2\text{O}_2$  and glucose, which has also been used in the successful detection of glucose in human serum. Results from this study not only demonstrate a new peroxidase mimic but also provide a novel ratiometric fluorescence platform for the detection of  $\text{H}_2\text{O}_2$  and metabolites involving reactions of  $\text{H}_2\text{O}_2$  generation in the absence of horseradish peroxidase.

**KEYWORDS:** *ion complexation, carbon nitride, peroxidase mimic, ratiometric fluorescence probe, hydrogen peroxide, glucose*

## 1. Introduction

Hydrogen peroxide ( $\text{H}_2\text{O}_2$ ) is a critical metabolite in cells and plays a vital role in physiological health. For instance,  $\text{H}_2\text{O}_2$  is a signal molecule related to oxidative stress and physiological activity.<sup>1</sup> An abnormal level of  $\text{H}_2\text{O}_2$  can increase the risk of central nervous system diseases and cancers.<sup>2</sup> Therefore, the detection of  $\text{H}_2\text{O}_2$  is of great significance for biomedical research and clinical diagnosis. Thus far, a range of techniques have been reported for  $\text{H}_2\text{O}_2$  detection, including electrochemistry,<sup>3</sup> colorimetry,<sup>4</sup> fluorescence,<sup>5</sup> and chemiluminescence.<sup>6</sup> Of these, the fluorescence method shows many advantages, such as rapid analysis, good sensitivity, and high selectivity. Compared with single fluorescence measurement, ratiometric fluorescence measurements can minimize erroneous signals from environmental influences and exhibit improved sensitivity and precision, because it is based on concurrent recording of two fluorescence signals at a single excitation wavelength.<sup>7</sup> For instance, ratiometric fluorescence detection of  $\text{H}_2\text{O}_2$  has been reported by using horseradish peroxidase (HRP) as the enzymatic catalyst.<sup>8-9</sup> In one study,<sup>8</sup> HRP catalyzes the oxidation of non-fluorescent *o*-phenylenediamine (OPD) to fluorescent 2,3-diaminophenazine (DAP), and DAP quenches the fluorescence of graphitic carbon nitride ( $\text{C}_3\text{N}_4$ ). These observations can be exploited for the construction of a ratiometric fluorescence platform for the detection of  $\text{H}_2\text{O}_2$  based on the decrease of the  $\text{C}_3\text{N}_4$  fluorescence and the enhancement of the DAP fluorescence. However, reports

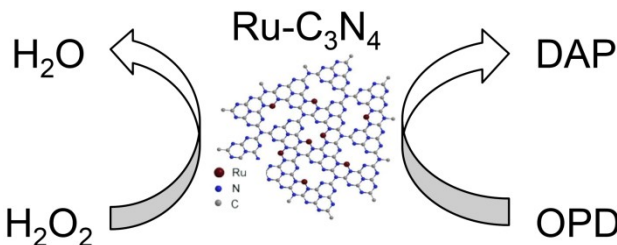
of ratiometric fluorescence detection of  $\text{H}_2\text{O}_2$  in the absence of HRP have been scarce. Notably, the use of peroxidase mimetics as the fluorescence probe may enable the detection of  $\text{H}_2\text{O}_2$  in the absence of HRP, which will be useful for living cell analysis in the future.

Enzyme mimetics hold great potential in replacing natural enzymes because of their low costs and high stability.<sup>10-11</sup> In 2007 magnetic  $\text{Fe}_3\text{O}_4$  nanoparticles were found to behave as peroxidase mimics.<sup>12</sup> Ever since, a vast variety of (nano)materials also exhibit peroxidase-like activities. These include noble metals,<sup>13-14</sup> metal oxides,<sup>15-17</sup> metal complexes,<sup>18-20</sup> and carbon materials<sup>21-22</sup>.  $\text{C}_3\text{N}_4$  and metal nanoparticles/ $\text{C}_3\text{N}_4$  composite materials have also been exploited as peroxidase mimetics for colorimetric detection of  $\text{H}_2\text{O}_2$ .<sup>23-25</sup> However, ratiometric fluorescence detection of  $\text{H}_2\text{O}_2$  has not been achieved based on peroxidase mimetics, which is anticipated to exhibit higher sensitivity and better selectivity than conventional colorimetric detection. This is the main motivation of the present work.

In an earlier study,<sup>26</sup> we demonstrated that the abundant pyridinic nitrogen of carbon nitride nanosheets could be exploited for the complexation of ruthenium(II) ions ( $\text{Ru-C}_3\text{N}_4$ ), which exhibited high electrocatalytic activity toward hydrogen evolution reaction. In the present study, it was found that  $\text{Ru-C}_3\text{N}_4$  also show high peroxidase-like activity, and might be exploited for the construction of a novel, effective ratiometric fluorescence platform for the detection of  $\text{H}_2\text{O}_2$  (**Scheme 1**). Experimentally, OPD was

oxidized by  $\text{H}_2\text{O}_2$  to produce DAP in the presence of  $\text{Ru-C}_3\text{N}_4$  (in place of HRP) that exhibited a fluorescence emission at 565 nm, and concurrently the fluorescence emission of  $\text{Ru-C}_3\text{N}_4$  (at 455 nm) was quenched by the generated DAP due to inner filter effect. The diminishment of the  $\text{Ru-C}_3\text{N}_4$  fluorescence together with the enhancement of the DAP fluorescence enables ratiometric fluorescence detection of  $\text{H}_2\text{O}_2$ . To the best of our knowledge, this is the first demonstration of peroxidase-like activity by  $\text{Ru-C}_3\text{N}_4$  nanocomposites and its use as a peroxidase-free ratiometric fluorescence probe for the detection of  $\text{H}_2\text{O}_2$ . The detection limit for  $\text{H}_2\text{O}_2$  (50 nM) is amongst the lowest ones reported previously, highlighting an effective strategy for the sensitive detection of  $\text{H}_2\text{O}_2$ . The unique property is also exploited for the sensitive and selective detection of glucose, which is known to generate  $\text{H}_2\text{O}_2$  when catalyzed by glucose oxidase (GOx).

**Scheme 1.** Schematic illustration of  $\text{Ru-C}_3\text{N}_4$  as a peroxidase mimic.



## 2. Experimental Section

**Chemicals.** Glucose oxidase (GOx, 150 kU g<sup>-1</sup>) was obtained from Sigma-Aldrich. Melamine, o-phenylenediamine (OPD), and hydrogen peroxide ( $\text{H}_2\text{O}_2$ , 30 wt.%) were purchased from Sinopharm Chemical Reagents Co. Ltd. Ruthenium(III) chloride ( $\text{RuCl}_3$ ), glucose, maltose, sucrose, galactose, bovine serum albumin (BSA), ascorbic acid, uric acid, and amino acids were purchased from Aladdin Chemicals Co., Ltd. Human serum samples were obtained from healthy volunteers in the Fourth Hospital of Changsha. All other reagents were of analytical or better grade and used as received. Acetate buffer solution was prepared with 0.10 M acetic acid and sodium acetate (pH 4.5). Phosphate buffer solution (PBS, pH 7.0) was prepared with 0.10 M  $\text{KH}_2\text{PO}_4$  and  $\text{Na}_2\text{HPO}_4$ . Water was purified with a Millipore Milli-Q System (resistivity 18.3 M $\Omega$ •cm).

**Preparation of  $\text{Ru-C}_3\text{N}_4$ .** The preparation of  $\text{Ru-C}_3\text{N}_4$  has been detailed previously.<sup>26</sup> Experimentally, graphitic  $\text{C}_3\text{N}_4$  nanosheets were first produced by thermal treatment of melamine in air followed by sonication in water.<sup>27-28</sup> (i) melamine (10 g) was loaded into a ceramic crucible with a cover, which was put into in a muffle furnace and heated at 600 °C for 3 h at the heating rate of 2.3 °C min<sup>-1</sup>, and (ii) 50 mg of the above products were dispersed into 50 mL of  $\text{H}_2\text{O}$ , and  $\text{C}_3\text{N}_4$  thin layers were formed by sonication overnight.

$\text{Ru-C}_3\text{N}_4$  was then prepared by thermal refluxing of the obtained  $\text{C}_3\text{N}_4$  and  $\text{RuCl}_3$  in water.<sup>26</sup> In brief, 56 mg of  $\text{RuCl}_3$  was added to the above  $\text{C}_3\text{N}_4$  dispersion, and the mixture was refluxed for 4 h. Centrifugation was then used

to separate the product, and excess ruthenium ions were removed by washing the collected solids with water and ethanol.

**Characterization.** High-resolution transmission electron microscopy (TEM) images were acquired with a TECNAI F-30 transmission electron microscope. X-ray photoelectron spectroscopy (XPS) studies were carried out with a Thermo Fisher XPS instrument. Ultraviolet-visible (UV-vis) absorption spectra were collected with a Shimadzu UV2450 spectrophotometer. Fluorescence spectroscopic studies were performed on a Hitachi F-7000 spectrophotometer. An Agilent 1260-7700e instrument was used for inductively coupled plasma-mass spectrometric (ICP-MS) analysis. Zeta potentials were evaluated with a Malvern Zetasizer Nano Z Analyzer.

**Detection of  $\text{H}_2\text{O}_2$ .** 10  $\mu\text{L}$  of a  $\text{H}_2\text{O}_2$  aqueous solution at different concentrations was added into 1 mL of the 0.10 M acetate buffer solution (pH 4.5) containing 50  $\mu\text{g mL}^{-1}$   $\text{Ru-C}_3\text{N}_4$  and 0.2 mM OPD. After incubation at 25 °C for 10 min, fluorescence measurements were carried out with the excitation set at 370 nm.

**Detection of glucose.** Experimentally, a 10  $\mu\text{L}$  solution containing 0.10 M PBS (pH 7.0), 0.50 mg  $\text{mL}^{-1}$  GOx and glucose of different concentrations was first prepared. After incubation at 25 °C for 30 min, the solution was transferred into 1 mL of the 0.10 M acetate buffer solution (pH 4.5) which contained 50  $\mu\text{g mL}^{-1}$   $\text{Ru-C}_3\text{N}_4$  and 0.2 mM OPD. Additional incubation was allowed for 10 min at 25 °C, before fluorescence spectra were acquired at 370 nm excitation. To detect glucose in human serum, the sample was diluted with PBS by a factor of 20, before fluorescence spectra were collected.

## 3. Results and Discussion

$\text{Ru-C}_3\text{N}_4$  was prepared by thermal refluxing of graphitic  $\text{C}_3\text{N}_4$  and  $\text{RuCl}_3$  in aqueous solution, where the ruthenium metal centers were incorporated within the  $\text{C}_3\text{N}_4$  scaffold by coordination to two pyridinic nitrogen moieties ( $\text{RuN}_2$ ), as described previously (Scheme 1).<sup>26</sup> The morphology of  $\text{Ru-C}_3\text{N}_4$  was first characterized by TEM measurements. As shown in Figure 1a-b,  $\text{Ru-C}_3\text{N}_4$  shows a nanosheet structure of a few tens of nanometer across, similar to that of pristine  $\text{C}_3\text{N}_4$  (Figure S1a). Figure 1c shows the high angle annular dark field scanning TEM (HAADF-STEM) image of  $\text{Ru-C}_3\text{N}_4$  and elemental maps based on energy-dispersive X-ray (EDX) analysis, where the C, N, Ru and Cl elements can be seen to be uniformly distributed in the sample. Note that no crystalline Ru species was found in  $\text{Ru-C}_3\text{N}_4$ , as demonstrated in high-resolution TEM and X-ray diffraction studies.<sup>26</sup> ICP-MS measurements showed that the Ru content in  $\text{Ru-C}_3\text{N}_4$  was ca. 9.97 at.%.

The chemical composition of  $\text{Ru-C}_3\text{N}_4$  was further examined by XPS measurements. From the survey spectrum in Figure 1d, one can readily identify the C, N, Ru, and Cl elements. Figure 1e shows the corresponding high-resolution spectrum of the Ru 3d and C 1s electrons. The Ru 3d<sub>5/2</sub> and 3d<sub>3/2</sub> electrons can be deconvoluted at 281.3 and 285.2 eV, which are consistent with those of Ru(II) in ruthenium bipyridine complexes,<sup>29</sup> suggesting that the Ru centers were mainly in the +2 valence state, as

detailed previously.<sup>26</sup> Two C 1s subpeaks can be found at 284.5 and 288.0 eV, which can be assigned to defective C in  $sp^3$  C-C and  $sp^2$ -hybridized C in N-C=N, respectively. Notably, the latter binding energy (288.0 eV for C in N-C=N) shows a marked blue shift for Ru-C<sub>3</sub>N<sub>4</sub>, as compared to that (287.3 eV) of pristine C<sub>3</sub>N<sub>4</sub> (**Figure S1b**), due to the formation of Ru-N coordination bonds.<sup>26</sup> Two nitrogen species can be identified from deconvolution of the N 1s peak for Ru-C<sub>3</sub>N<sub>4</sub>, the  $sp^3$ -hybridized tertiary N (N-(C)<sub>3</sub>) at 399.7 eV and the  $sp^2$ -hybridized pyridinic N (C-N=C) at 398.4 eV (**Figure 1f**). Again, because of ruthenium ion complexation, the binding energy of N in N-C=N for Ru-C<sub>3</sub>N<sub>4</sub> is higher than that for pristine C<sub>3</sub>N<sub>4</sub> (397.8 eV, **Figure S1c**). The Cl 2p peak for Ru-C<sub>3</sub>N<sub>4</sub> in **Figure 1g** is fitted with Cl 2p<sub>3/2</sub> at 199.2 eV and Cl 2p<sub>1/2</sub> at 197.6 eV, indicating the presence of chloride ions in outer-sphere to neutralize the charge. These results are consistent with those obtained previously.<sup>26</sup> In addition, the atomic ratio of C/N in both C<sub>3</sub>N<sub>4</sub> and Ru-C<sub>3</sub>N<sub>4</sub> is found to be close to 3:4 by elemental analysis (**Table S1**).

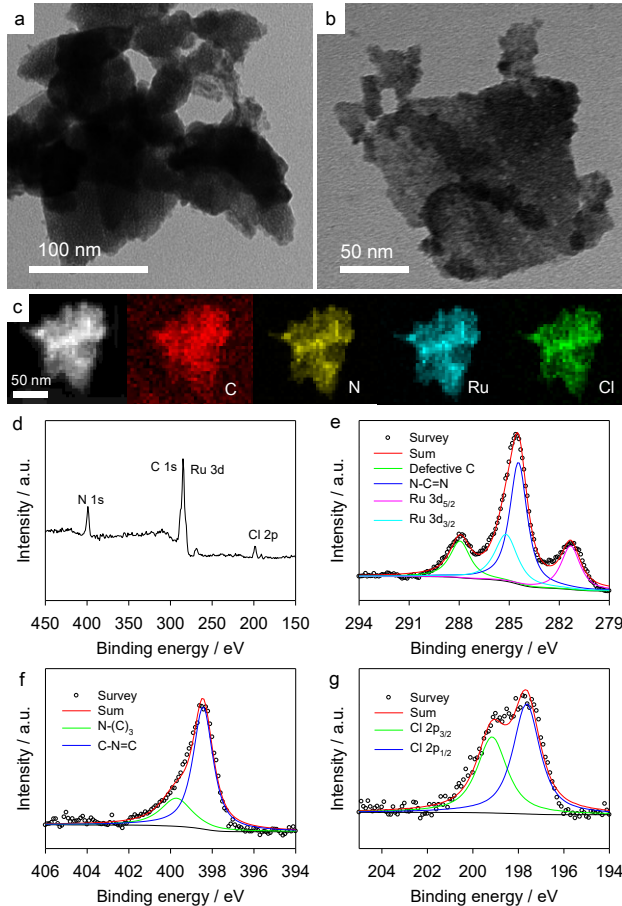


**Figure 1.** (a, b) Representative TEM images, (c) HAADF-STEM image and elemental maps, and (d) XPS survey spectrum of Ru-C<sub>3</sub>N<sub>4</sub>. High-resolution XPS scans of the (e) Ru 3d and C 1s, (f) N 1s, and (g) Cl 2p electrons in Ru-C<sub>3</sub>N<sub>4</sub>.

The catalytic activity of Ru-C<sub>3</sub>N<sub>4</sub> towards the oxidation of peroxidase substrate OPD in the presence of H<sub>2</sub>O<sub>2</sub> was then tested in the acetate buffer (pH 4.5) at 25 °C. After incubation of the solution containing 0.2 mM OPD, 1 mM H<sub>2</sub>O<sub>2</sub> and 50  $\mu$ g mL<sup>-1</sup> Ru-C<sub>3</sub>N<sub>4</sub> for 10 min, the solution was found to exhibit a yellow color (**Figure 2a**) with a sharp absorption peak at 450 nm (**Figure 2b**), indicating

effective catalysis of the oxidation of OPD to yellow DAP by Ru-C<sub>3</sub>N<sub>4</sub> in the presence of H<sub>2</sub>O<sub>2</sub> (**Scheme 1**). By contrast, in the absence of Ru-C<sub>3</sub>N<sub>4</sub> or H<sub>2</sub>O<sub>2</sub>, the solution remained colorless (**Figure 2a**), and exhibited no apparent absorption peak at 450 nm (**Figure 2b**), suggesting that the direct oxidation of OPD by Ru-C<sub>3</sub>N<sub>4</sub> or H<sub>2</sub>O<sub>2</sub> alone was kinetically sluggish. Note that whereas C<sub>3</sub>N<sub>4</sub> has been reported to show peroxidase-like activity,<sup>23</sup> we found that this catalytic activity was markedly lower than that of Ru-C<sub>3</sub>N<sub>4</sub> under the same reaction conditions. As the peroxidase-like activity of Ru-C<sub>3</sub>N<sub>4</sub> reached the maximum at pH 4.5 (**Figure S2**), all the catalytic experiments were conducted in the 0.10 mM acetate buffer (pH 4.5).

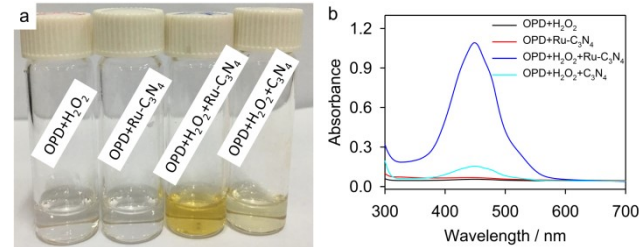


**Figure 2.** (a) Photograph and (b) UV-vis absorption spectra of OPD+H<sub>2</sub>O<sub>2</sub>, OPD+Ru-C<sub>3</sub>N<sub>4</sub>, OPD+H<sub>2</sub>O<sub>2</sub>+Ru-C<sub>3</sub>N<sub>4</sub>, and OPD+H<sub>2</sub>O<sub>2</sub>+C<sub>3</sub>N<sub>4</sub>. Experiments are carried out in 0.1 mM acetate buffer (pH 4.5) containing 0.2 mM OPD, 1 mM H<sub>2</sub>O<sub>2</sub>, 50  $\mu$ g mL<sup>-1</sup> Ru-C<sub>3</sub>N<sub>4</sub>, and 50  $\mu$ g mL<sup>-1</sup> C<sub>3</sub>N<sub>4</sub>.

The steady-state kinetic parameters for OPD and H<sub>2</sub>O<sub>2</sub> in the catalytic reaction were then quantitatively evaluated. From the Michaelis-Menten and Lineweaver-Burk plots in **Figure S3**, the Michaelis constant ( $K_m$ ) and maximal reaction velocity ( $V_{max}$ ) for Ru-C<sub>3</sub>N<sub>4</sub> toward OPD were estimated to be 0.068 mM and 8.33  $\mu$ M s<sup>-1</sup>, respectively. The small  $K_m$  value indicates that Ru-C<sub>3</sub>N<sub>4</sub> possessed a high binding affinity toward H<sub>2</sub>O<sub>2</sub>, while the large  $V_{max}$  value indicates that Ru-C<sub>3</sub>N<sub>4</sub> exhibited a high catalytic activity. Similarly, for Ru-C<sub>3</sub>N<sub>4</sub> toward H<sub>2</sub>O<sub>2</sub> (**Figure S4**),  $K_m$  is estimated to be 2.4 mM and  $V_{max}$  41.66  $\mu$ M s<sup>-1</sup>. The  $K_m$  value toward H<sub>2</sub>O<sub>2</sub> for Ru-C<sub>3</sub>N<sub>4</sub> is much smaller than those for Ru frames (318 mM),<sup>30</sup> Pd nanoplates (4.4 mM),<sup>31</sup> and Fe<sub>3</sub>O<sub>4</sub> nanoparticles (154 mM),<sup>12</sup> suggesting that the Ru-C<sub>3</sub>N<sub>4</sub> has higher binding affinity toward H<sub>2</sub>O<sub>2</sub> than the other peroxidase mimetics reported previously. Furthermore, the  $V_{max}$  value toward H<sub>2</sub>O<sub>2</sub> for Ru-C<sub>3</sub>N<sub>4</sub> is much larger than those for peroxidase mimetics reported previously (4.45  $\mu$ M s<sup>-1</sup> for Ru frames,<sup>30</sup> 3.906  $\mu$ M s<sup>-1</sup> for Pd nanoplates,<sup>31</sup> and 5.868  $\mu$ M s<sup>-1</sup> for Fe<sub>3</sub>O<sub>4</sub> nanoparticles),<sup>12</sup> signifying the high peroxidase-like activity of Ru-C<sub>3</sub>N<sub>4</sub>. In addition to the high catalytic activity, Ru-C<sub>3</sub>N<sub>4</sub> also showed excellent stability. After storage at ambient temperature for half a year, the catalytic activity of Ru-C<sub>3</sub>N<sub>4</sub> was found to remain virtually unchanged.

The fluorescence property of Ru-C<sub>3</sub>N<sub>4</sub> was further examined. From **Figure S5a**, Ru-C<sub>3</sub>N<sub>4</sub> can be seen to exhibit an excitation peak at 370 nm and an emission peak at 455 nm; and at 370 nm excitation, the 455 nm fluorescence emission increases proportionally to the concentration of Ru-C<sub>3</sub>N<sub>4</sub> (**Figure S5b**). Yet, from **Figure 3a**, one can see that this emission is markedly quenched after incubation of 50  $\mu$ g mL<sup>-1</sup> Ru-C<sub>3</sub>N<sub>4</sub> with 0.2 mM OPD

and 1 mM H<sub>2</sub>O<sub>2</sub> in 0.1 mM acetate buffer (pH 4.5) at 25 °C for 10 min. In addition, a new fluorescence peak emerges at 565 nm. This is due to the oxidation of OPD to fluorescent DAP catalysed by Ru-C<sub>3</sub>N<sub>4</sub> in the presence of H<sub>2</sub>O<sub>2</sub>. By contrast, OPD or H<sub>2</sub>O<sub>2</sub> alone shows no influence on the fluorescence of Ru-C<sub>3</sub>N<sub>4</sub>.

To reveal the mechanism of the quenching of Ru-C<sub>3</sub>N<sub>4</sub> fluorescence, the lifetime of Ru-C<sub>3</sub>N<sub>4</sub> emission was measured and compared in the absence and presence of DAP. From **Figure 3b**, it can be seen that the fluorescence decay profiles of Ru-C<sub>3</sub>N<sub>4</sub> remain virtually unchanged before and after the quenching by DAP, indicating no energy or electron transfer between Ru-C<sub>3</sub>N<sub>4</sub> and DAP. Additionally, as the zeta potentials of Ru-C<sub>3</sub>N<sub>4</sub>, OPD and DAP are all positive in 0.10 mM acetate buffer (pH 4.5) (**Figure S6**), it is unlikely that Förster resonance energy transfer occurred, because of electrostatic repulsion between Ru-C<sub>3</sub>N<sub>4</sub> and DAP. From **Figure S7**, one can see that there is a substantial overlap around 450 nm between the absorption spectrum of DAP and the fluorescence emission spectrum of Ru-C<sub>3</sub>N<sub>4</sub> (at 370 nm excitation), so the quenching of Ru-C<sub>3</sub>N<sub>4</sub> by DAP most likely arose from the inner filter effect.

Taken together, the experimental results presented above suggest that Ru-C<sub>3</sub>N<sub>4</sub> exhibits apparent peroxidase-like activity and can catalyze the oxidation of OPD to fluorescent DAP in the presence of H<sub>2</sub>O<sub>2</sub> as a peroxidase mimic. As the fluorescence of Ru-C<sub>3</sub>N<sub>4</sub> is concurrently quenched by the generated DAP due to inner filter effect, Ru-C<sub>3</sub>N<sub>4</sub> can be exploited as an effective ratiometric fluorescence probe for the detection of H<sub>2</sub>O<sub>2</sub>. To achieve high ratiometric response toward H<sub>2</sub>O<sub>2</sub>, several important parameters were optimized (**Figure S8**), i.e., Ru-C<sub>3</sub>N<sub>4</sub> concentration 50 µg mL<sup>-1</sup>, OPD concentration 0.2 mM, solution pH 4.5, and incubation time 10 min.

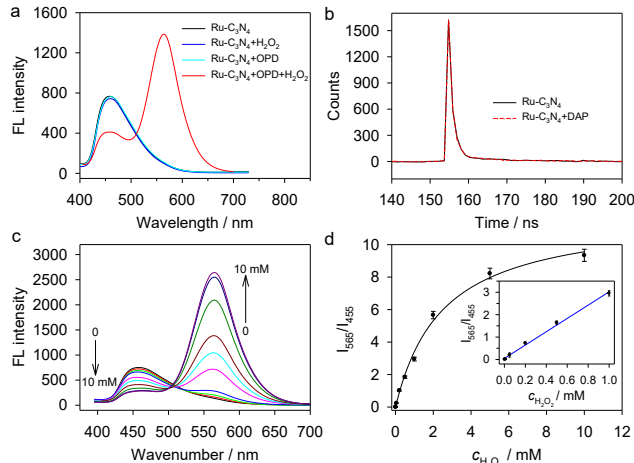


**Figure 3.** (a) Fluorescence emission spectra of Ru-C<sub>3</sub>N<sub>4</sub>, Ru-C<sub>3</sub>N<sub>4</sub>+H<sub>2</sub>O<sub>2</sub>, Ru-C<sub>3</sub>N<sub>4</sub>+OPD, and Ru-C<sub>3</sub>N<sub>4</sub>+OPD+H<sub>2</sub>O<sub>2</sub> at 370 nm excitation. Experiments are carried out in 0.1 mM acetate buffer (pH 4.5) for 10 min at 25 °C with 0.2 mM OPD, 1 mM H<sub>2</sub>O<sub>2</sub>, and 50 µg mL<sup>-1</sup> Ru-C<sub>3</sub>N<sub>4</sub>. (b) Time-resolved fluorescence spectra of Ru-C<sub>3</sub>N<sub>4</sub> in the absence and presence of DAP. (c) Fluorescence spectra of Ru-C<sub>3</sub>N<sub>4</sub>-based ratiometric fluorescence probe at 370 nm excitation in the presence of H<sub>2</sub>O<sub>2</sub> at different concentrations. (d) Ratiometric fluorescence intensity (I<sub>565</sub>/I<sub>455</sub>) versus H<sub>2</sub>O<sub>2</sub> concentration. Inset shows the linear range.

(calibration curve) for the detection of H<sub>2</sub>O<sub>2</sub>, where symbols are experimental data and line is linear regression.

Under these optimized experimental conditions, the Ru-C<sub>3</sub>N<sub>4</sub> based ratiometric sensing platform was evaluated by fluorescence measurements, where emission spectra were recorded at the excitation wavelength of 370 nm in the presence of H<sub>2</sub>O<sub>2</sub> at different concentrations. From **Figure 3c**, one can see that with the increase of the H<sub>2</sub>O<sub>2</sub> concentration, the fluorescence emission intensity of Ru-C<sub>3</sub>N<sub>4</sub> at 455 nm decreases accordingly, whereas the fluorescence emission of DAP at 565 nm becomes intensified. **Figure 3d** shows the variation of the ratiometric fluorescence intensity (I<sub>565</sub>/I<sub>455</sub>) with H<sub>2</sub>O<sub>2</sub> concentration, where the linear range for H<sub>2</sub>O<sub>2</sub> detection is estimated from 2 × 10<sup>-4</sup> to 1.0 mM (inset to **Figure 3d**), with a linear regression equation of  $y = 0.0502 + 2.97x$  ( $R^2 = 0.9955$ ). The detection limit (3σ/k, with k being the slope of the curve and σ the standard deviation) is 50 nM, which is lower than results in leading studies reported in recent literature (**Table S2**). Additionally, from **Figure S9**, other biologically relevant radicals (e.g., OH<sup>•</sup>, ClO<sup>•</sup>, O<sub>2</sub><sup>•</sup>, and ONOO<sup>•</sup>) can be seen to display no obvious influence on the ratiometric fluorescence detection of H<sub>2</sub>O<sub>2</sub>, indicating that Ru-C<sub>3</sub>N<sub>4</sub>-based ratiometric sensing system has good specificity toward H<sub>2</sub>O<sub>2</sub>.

Since Ru-C<sub>3</sub>N<sub>4</sub> shows apparent activity as a ratiometric fluorescence probe for H<sub>2</sub>O<sub>2</sub> detection, it may be exploited further as a universal platform for the detection of metabolites that can generate H<sub>2</sub>O<sub>2</sub> when catalyzed by enzymes in the human body. In this work, glucose was selected as the model target, as H<sub>2</sub>O<sub>2</sub> can be readily produced from glucose using GOx as the catalyst. Experimentally, the optimal GOx concentration was ca. 0.5 mg mL<sup>-1</sup>, with an incubation time of 30 min for glucose with GOx (**Figure S10**). From **Figure 4a**, it can be seen that at increasing glucose concentrations, the intensity of the fluorescence emission of Ru-C<sub>3</sub>N<sub>4</sub> at 455 nm decreases accordingly, while the fluorescence emission of DAP at 565 nm increases concurrently. **Figure 4b** shows the ratiometric fluorescence intensity (I<sub>565</sub>/I<sub>455</sub>) at different glucose concentrations, which features a linear range for glucose detection from 1 × 10<sup>-3</sup> to 0.5 mM (**Figure 4c**), with a linear regression equation of  $y = 0.0721 + 2.26x$  ( $R^2 = 0.9936$ ). The detection limit is evaluated to be ca. 0.1 µM, which, again, is better than leading literature results (**Table S3**).

The selectivity of the Ru-C<sub>3</sub>N<sub>4</sub> based ratiometric sensing system was then investigated. From **Figure 4d**, no apparent influence was observed on the ratiometric fluorescence detection of glucose in the presence of a variety of potential interferents, such as maltose, galactose, sucrose, fructose, ascorbic acid, uric acid, lysine, glycine, and (transition) metal ions (e.g., Fe<sup>3+</sup>, Cu<sup>2+</sup>, Mg<sup>2+</sup>, Ca<sup>2+</sup>, and K<sup>+</sup>), suggesting excellent selectivity and GOx-like catalytic specificity of Ru-C<sub>3</sub>N<sub>4</sub>. The Ru-C<sub>3</sub>N<sub>4</sub> based ratiometric fluorescence probe was further tested for detecting glucose in human serum. As shown in **Table S4**, the performance of Ru-C<sub>3</sub>N<sub>4</sub> was highly comparable to that of a commercial glucometer. The recovery efficiencies were between 95.5% and 104.3%, and the relative standard deviations from 2.2% to 4.5%. These results suggest that the Ru-C<sub>3</sub>N<sub>4</sub> based ratiometric

sensing probe is capable of glucose detection in human serum.

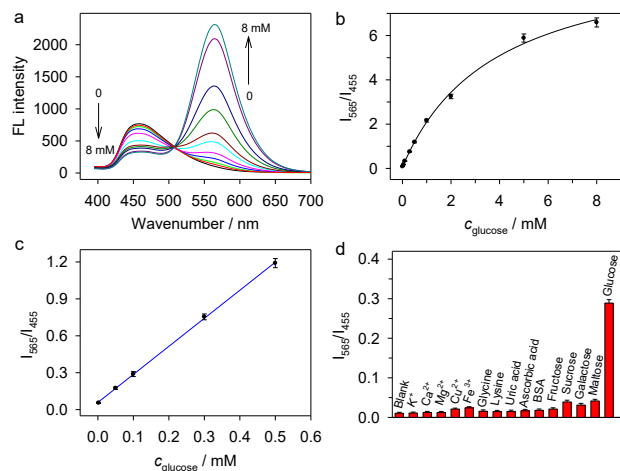


**Figure 4.** (a) Fluorescence emission spectra of Ru-C<sub>3</sub>N<sub>4</sub> based ratiometric fluorescence probe at 370 nm excitation in the presence of glucose at different concentrations. (b) Ratiometric fluorescence intensity ( $I_{565}/I_{455}$ ) versus glucose concentration. (c) Linear range (calibration curve) for the detection of glucose. (d) Selectivity of glucose detection. The concentration of glucose is 0.10 mM, BSA 1 mg mL<sup>-1</sup>, and all other interferents 1 mM

## 4. Conclusion

In conclusion, Ru-C<sub>3</sub>N<sub>4</sub> nanosheets were found to display apparent peroxidase-like activity and behave as a peroxidase mimic to catalyze the oxidation of OPD to fluorescent DAP in the presence of H<sub>2</sub>O<sub>2</sub>. As the fluorescence emission of Ru-C<sub>3</sub>N<sub>4</sub> was concurrently quenched by the produced DAP by virtue of the inner filter effect, an effective ratiometric fluorescence platform was constructed for the detection of H<sub>2</sub>O<sub>2</sub> and glucose. The detection limit was estimated to be 50 nM for H<sub>2</sub>O<sub>2</sub> and 0.1  $\mu\text{M}$  for glucose. Notably, the sensing platform was successfully used for detecting glucose in human serum, highlighting the significant potential in the sensitive detection of metabolites involving H<sub>2</sub>O<sub>2</sub>-generation reactions.

## ASSOCIATED CONTENT

### Supporting Information

The Supporting Information is available free of charge on the ACS Publications website.

Additional experimental data: TEM and XPS characterization of C<sub>3</sub>N<sub>4</sub> (Figure S1), peroxidase-like activity of Ru-C<sub>3</sub>N<sub>4</sub> at different solution pH (Figure S2), kinetic investigation of Ru-C<sub>3</sub>N<sub>4</sub> toward OPD (Figure S3), kinetic investigation of Ru-C<sub>3</sub>N<sub>4</sub> toward H<sub>2</sub>O<sub>2</sub> (Figure S4), fluorescence spectra of Ru-C<sub>3</sub>N<sub>4</sub> (Figure S5), Zeta potentials of Ru-C<sub>3</sub>N<sub>4</sub>, OPD, and DAP (Figure S6), UV-Vis absorption spectrum of DAP and fluorescence emission spectrum of Ru-C<sub>3</sub>N<sub>4</sub> (Figure S7), optimization of experimental parameters for H<sub>2</sub>O<sub>2</sub> detection (Figure S8), selectivity of H<sub>2</sub>O<sub>2</sub> detection (Figure S9), optimization of experimental parameters for glucose detection of (Figure S10), elemental analysis results (Table S1), performance comparison of H<sub>2</sub>O<sub>2</sub> detection (Table S2), performance comparison of glucose detection (Table S3), and comparison of glucose detection in human serum with a commercial glucometer (Table S4).

## AUTHOR INFORMATION

### Corresponding Authors

\* tanyueming0813@126.com; tanyueming0813@hunnu.edu.cn; shaowei@ucsc.edu

### Author Contributions

The manuscript was written through contributions of all authors. All authors have given approval to the final version of the manuscript.

‡ These authors contributed equally to the work.

## ACKNOWLEDGMENT

Work at HNNU was supported by the National Natural Science Foundation of China (21705045 and 21775041), the Science and Technology Innovation Project of Hunan Province (2018RS3062), the Natural Science Foundation of Hunan Province (2018JJ2252), the Scientific Research Fund of Hunan Provincial Education Department (17A125), and the Science and Technology Project of Changsha (KQ1802036). Work at UCSC was supported by the National Science Foundation through grants CHE-1710408 and CBET-1848841. W.F.D. and Y.M.T. were supported by a fellowship from the China Scholarship Council.

## REFERENCES

- Lin, M. T.; Beal, M. F., Mitochondrial Dysfunction and Oxidative Stress in Neurodegenerative Diseases. *Nature* **2006**, *443*, 787-795.
- Finkel, T.; Serrano, M.; Blasco, M. A., The Common Biology of Cancer and Ageing. *Nature* **2007**, *448*, 767-774.
- Li, Z.; Xin, Y.; Wu, W.; Fu, B.; Zhang, Z., Topotactic Conversion of Copper(I) Phosphide Nanowires for Sensitive Electrochemical Detection of H<sub>2</sub>O<sub>2</sub> Release from Living Cells. *Anal. Chem* **2016**, *88*, 7724-7729.
- Narayanaswamy, N.; Narra, S.; Nair, R. R.; Saini, D. K.; Kondaiah, P.; Govindaraju, T., Stimuli-Responsive Colorimetric and NIR Fluorescence Combination Probe for Selective Reporting of Cellular Hydrogen Peroxide. *Chem. Sci.* **2016**, *7*, 2832-2841.
- Abo, M.; Urano, Y.; Hanaoka, K.; Terai, T.; Komatsu, T.; Nagano, T., Development of a Highly Sensitive Fluorescence Probe for Hydrogen Peroxide. *J. Am. Chem. Soc.* **2011**, *133*, 10629-10637.
- Zhu, Q.; Huang, J.; Yan, M.; Ye, J.; Wang, D.; Lu, Q.; Yang, X., N-(Aminobutyl)-N-(ethylsulfonyl)-Functionalized Gold Nanoparticles on Cobalt Disulfide Nanowire Hybrids for the Non-Enzymatic Chemiluminescence Detection of H<sub>2</sub>O<sub>2</sub>. *Nanoscale* **2018**, *10* 14847-14851.
- Ajayaghosh, A.; Carol, P.; Sreejith, S., A Ratiometric Fluorescence Probe for Selective Visual Sensing of Zn<sup>2+</sup>. *J. Am. Chem. Soc.* **2005**, *127*, 14962-14963.
- Liu, J.-W.; Luo, Y.; Wang, Y.-M.; Duan, L.-Y.; Jiang, J.-H.; Yu, R.-Q., Graphitic Carbon Nitride Nanosheets-Based Ratiometric Fluorescent Probe for Highly Sensitive Detection of H<sub>2</sub>O<sub>2</sub> and Glucose. *ACS Appl. Mater. Interfaces* **2016**, *8*, 33439-33445.
- Ma, Y.; Cen, Y.; Sohail, M.; Xu, G.; Wei, F.; Shi, M.; Xu, X.; Song, Y.; Ma, Y.; Hu, Q., A Ratiometric Fluorescence Universal Platform Based on N, Cu Codoped Carbon Dots to Detect Metabolites Participating in H<sub>2</sub>O<sub>2</sub>-Generation Reactions. *ACS Appl. Mater. Interfaces* **2017**, *9*, 33011-33019.
- Lin, Y.; Ren, J.; Qu, X., Catalytically Active Nanomaterials: A Promising Candidate for Artificial Enzymes. *Acc. Chem. Res.* **2014**, *47*, 1097-1105.
- Wei, H.; Wang, E., Nanomaterials with Enzyme-Like Characteristics (Nanozymes): Next-Generation Artificial Enzymes. *Chem. Soc. Rev.* **2013**, *42*, 6060-6093.
- Gao, L.; Zhuang, J.; Nie, L.; Zhang, J.; Zhang, Y.; Gu, N.; Wang, T.; Feng, J.; Yang, D.; Perrett, S.; Yan, X., Intrinsic Peroxidase-Like Activity of Ferromagnetic Nanoparticles. *Nat. Nanotechnol.* **2007**, *2*, 577-583

13. Jv, Y.; Li, B. X.; Cao, R., Positively-Charged Gold Nanoparticles as Peroxidase Mimic and Their Application in Hydrogen Peroxide and Glucose Detection. *Chem. Commun.* **2010**, *46*, 8017-8019.

14. He, W. W.; Wu, X. C.; Liu, J. B.; Hu, X. N.; Zhang, K.; Hou, S.; Zhou, W. Y.; Xie, S. S., Design of AgM Bimetallic Alloy Nanostructures (M = Au, Pd, Pt) with Tunable Morphology and Peroxidase-like Activity. *Chem. Mater.* **2010**, *22*, 2988-2994.

15. Andre, R.; Natalio, F.; Humanes, M.; Leppin, J.; Heinze, K.; Wever, R.; Schroder, H. C.; Muller, W. E. G.; Tremel, W., V<sub>2</sub>O<sub>5</sub> Nanowires with an Intrinsic Peroxidase-like Activity. *Adv. Funct. Mater.* **2011**, *21*, 501-509.

16. Mu, J. S.; Wang, Y.; Zhao, M.; Zhang, L., Intrinsic Peroxidase-like Activity and Catalase-like Activity of Co<sub>3</sub>O<sub>4</sub> Nanoparticles. *Chem. Commun.* **2012**, *48*, 2540-2542.

17. Liu, J.; Meng, L. J.; Fei, Z. F.; Dyson, P. J.; Jing, X. N.; Liu, X., MnO<sub>2</sub> Nanosheets as an Artificial Enzyme to Mimic Oxidase for Rapid and Sensitive Detection of Glutathione. *Biosens. Bioelectron.* **2017**, *90*, 69-74.

18. Wang, S.; Deng, W.; Yang, L.; Tan, Y.; Xie, Q.; Yao, S., Copper-Based Metal-Organic Framework Nanoparticles with Peroxidase-Like Activity for Sensitive Colorimetric Detection of *Staphylococcus aureus*. *ACS Appl. Mater. Interfaces* **2017**, *9*, 24440-24445.

19. Zhang, J. W.; Zhang, H. T.; Du, Z. Y.; Wang, X.; Yu, S. H.; Jiang, H. L., Water-Stable Metal-Organic Frameworks with Intrinsic Peroxidase-Like Catalytic Activity as a Colorimetric Biosensing Platform. *Chem. Commun.* **2014**, *50*, 1092-1094.

20. Vázquez-González, M.; Liao, W.-C.; Cazelles, R. m.; Wang, S.; Yu, X.; Gutkin, V.; Willner, I., Mimicking Horseradish Peroxidase Functions Using Cu<sup>2+</sup>-Modified Carbon Nitride Nanoparticles or Cu<sup>2+</sup>-Modified Carbon Dots as Heterogeneous Catalysts. *ACS Nano* **2017**, *11*, 3247-3253.

21. Song, Y.; Qu, K.; Zhao, C.; Ren, J.; Qu, X., Graphene Oxide: Intrinsic Peroxidase Catalytic Activity and Its Application to Glucose Detection. *Adv. Mater.* **2010**, *22*, 2206 - 2210.

22. Wang, Y.-M.; Liu, J.-W.; Adkins, G. B.; Shen, W.; Trinh, M. P.; Duan, L.-Y.; Jiang, J.-H.; Zhong, W., Enhancement of the Intrinsic Peroxidase-Like Activity of Graphitic Carbon Nitride Nanosheets by ssDNAs and Its Application for Detection of Exosomes. *Anal. Chem.* **2017**, *89*, 12327-12333.

23. Lin, T.; Zhong, L.; JingWang; Guo, L.; Wu, H.; Guo, Q.; Fu, F.; Chen, G., Graphite-Like Carbon Nitrides as Peroxidase Mimetics and Their Applications to Glucose Detection. *Biosens. Bioelectron.* **2014**, *59*, 89-93.

24. Wang, N.; Han, Z.; Fan, H.; Ai, S., Copper Nanoparticles Modified Graphitic Carbon Nitride Nanosheets as a Peroxidase Mimetic for Glucose Detection. *RSC Adv.* **2015**, *5*, 91302-91307.

25. Darabdhara, G.; Bordoloi, J.; Manna, P.; Das, M., R. Biocompatible Bimetallic Au-Ni Doped Graphitic Carbon Nitride Sheets: A Novel Peroxidase-Mimicking Artificial Enzyme for Rapid and Highly Sensitive Colorimetric Detection of Glucose. *Sens. Actuat. B-Chem.* **2019**, *285*, 277-290.

26. Peng, Y.; Lu, B.; Chen, L.; Wang, N.; Lu, J. E.; Ping, Y.; Chen, S., Hydrogen Evolution Reaction Catalyzed by Ruthenium Ion-Complexed Graphitic Carbon Nitride Nanosheets. *J. Mater. Chem. A* **2017**, *5*, 18261-18269.

27. Tian, J.; Liu, Q.; Ge, C.; Xing, Z.; Asiri, A. M.; Al-Youbi, A. O.; Sun, X., Ultrathin graphitic carbon nitride nanosheets: a low-cost, green, and highly efficient electrocatalyst toward the reduction of hydrogen peroxide and its glucose biosensing application. *Nanoscale* **2013**, *5*, 8921-8924.

28. Zhang, X.; Xie, X.; Wang, H.; Zhang, J.; Pan, B.; Xie, Y., Enhanced photoresponsive ultrathin graphitic-phase C<sub>3</sub>N<sub>4</sub> nanosheets for bioimaging. *J. Am. Chem. Soc.* **2013**, *135*, 18-21.

29. Agnès, C.; Arnault, J.-C.; Omnès, F.; Joussetme, B.; Billon, M.; Bidan, G.; Mailley, P., XPS Study of Ruthenium Tris-Bipyridine Electrografted from Diazonium Salt Derivative on Microcrystalline Boron Doped Diamond. *Phys. Chem. Chem. Phys* **2009**, *11*, 11647-11654.

30. Ye, H.; Mohar, J.; Wang, Q.; Catalano, M.; Kim, M. J.; Xia, X., Peroxidase-Like Properties of Ruthenium Nanoframes. *Science Bulletin* **2016**, *61*, 1739-1745.

31. Wei, J.; Chen, X.; Shi, S.; Mo, S.; Zheng, N., An Investigation of the Mimetic Enzyme Activity of Two-Dimensional Pd-Based Nanostructures. *Nanoscale* **2015**, *7*, 19018-19026.

## TOC Graph

